Effect of Seismic Waves with Different Dominant Frequencies on the Delayed Failure Behavior of a Soil Structure-Ground System

Effets des ondes sismiques de fréquence dominante différente sur le comportement de rupture retardée de structures en terre et de systèmes de sol

Shimizu R., Yamada S.
Nagoya University, Japan

ABSTRACT: In this research, a method of obtaining the natural frequencies and natural frequency modes was derived for a soil-water 2-phase system initial value/boundary value problem. Using this method, the natural frequencies and natural frequency modes of the whole soil structure-ground system were calculated for the ground and an embankment constructed on it. The modes extracted included (1) modes in which the ground deformed greatly and (2) modes in which the soil structure deformed greatly. In addition, seismic response analysis was carried out by inputting two types of seismic wave having dominant frequencies close to the natural frequencies corresponding to each mode. The results showed that delayed failure behavior progressing from the ground into the soil structure was exhibited for the seismic waves that targeted (1) and that delayed failure behavior progressing from the soil structure to the ground was exhibited for the seismic waves that targeted (2).

RÉSUMÉ : Cette étude se propose de dériver une méthode de calcul de la fréquence propre et du mode propre de vibration pour le problème de la valeur initiale et de la valeur limite d'un système squelette eau-sol à deux phases. À l'aide de cette méthode appliquée à des remblais créer sur un sol nous avons déterminé (1) un mode où le sol se déforme considérablement (2) un mode où les structures de terre se déforment considérablement, en calculant la fréquence propre et le mode propre de vibration présismique du système structures de terre-sol global. Nous avons par ailleurs analysé la réponse sismique en entrant deux types d'ondes sismiques possédant une fréquence prédominante au voisinage de la fréquence propre pour chacun des modes pour amplifier chacun de ceux-ci. Les résultats montrent l'apparition de comportements de rupture différée qui se propagent du sol à la structure de terre pour les ondes sismiques en (1), et l'apparition de comportements de rupture différée qui se propagent de la structure en terre au sol pour les ondes sismiques en (2).

KEYWORDS: natural frequency analysis, seismic response analysis, soil-water coupled finite deformation analysis.

1 INTRODUCTION

In this paper, we propose a method for evaluating the natural frequency and natural frequency mode in the context of an initial-boundary value problem of a two-phase soil-water system. In addition, we calculate the natural frequency and natural frequency mode of the entire soil structure-ground system immediately before the simulated earthquake, specifically that of an embankment and the ground on which it is built, and determine the mode for which the ground and embankment undergo large-scale deformation. Further, we input two types of seismic waves with dominant frequencies close to the natural frequencies of each mode, analyze the seismic response using the soil-water coupled finite deformation analysis code ***GEOASIA*** (Noda et al. 2008a), and thereby demonstrate that differences in the dominant natural frequency mode substantially impact the deformation/failure behavior of the soil structure-ground system.

2 FORMULARIZATION OF A FINITE ELEMENT DISCRETIZED RATE-TYPE EQUATION OF MOTION AND SOIL-WATER COUPLED EQUATION AS AN EIGENVALUE PROBLEM

In dynamic initial-boundary value problems for elasto-plastic materials that can be described by a rate-type constitutive equation, it is necessary to solve a rate-type equation of motion. To this end, after deriving a weak form of the rate-type equation of motion, we employ an elasto-plastic constitutive equation formulated with effective stress as the constitutive equation for the soil skeleton and perform finite element discretization. Furthermore, we represent the pore water pressure u at the center of each element in the soil-water coupled equation by extending the physical models of Christian (1968) or Akai & Tamura (1978) to the continuity equation for saturated soil or the equation for the average flow velocity of pore water. Moreover, when the viscous boundary or linear constraint conditions (Asaoka et al. 1998) on velocity field of nodes are applied, the final system of simultaneous ordinary differential equations to be solved is as follows (Noda et al. 2008a):

$$\left.\begin{aligned} &[\mathrm{M}]\{\ddot{\boldsymbol{v}}\} + [\mathrm{C}^*]\{\dot{\boldsymbol{v}}\} + [\mathrm{K}]\{\boldsymbol{v}\} - [\mathrm{L}]^{\mathrm{T}}\{\dot{u}\} - [\mathrm{C}]^{\mathrm{T}}\{\dot{\mu}\} = \{\dot{\boldsymbol{f}}\} \\ &[\mathrm{L}']\{\dot{\boldsymbol{v}}\} - [\mathrm{L}]\{\boldsymbol{v}\} + [\mathrm{H}]\{u\} + [\mathrm{G}]\{\dot{u}\} = \{f_u\} \\ &-[\mathrm{C}]\{\boldsymbol{v}\} = \{0\} \end{aligned}\right\} \quad (1)$$

where $[\mathrm{M}]$ is the mass matrix, $[\mathrm{K}]$ is the tangential stiffness matrix, $[\mathrm{L}]$ is a matrix for converting displacement velocities of the soil skeleton to a volumetric change rate of the soil skeleton, $\{\boldsymbol{v}\}$ is a vector comprising the displacement velocities of nodes, $\{\dot{u}\}$ is the pore water pressure rate at the center of each element as seen from the soil skeleton, $[\mathrm{L}']$ is a matrix for the acceleration term of the soil-water coupled equation derived from $[\mathrm{L}]$, $[\mathrm{H}]$ is the permeability matrix, and $[\mathrm{G}]$ is the matrix for porosity and water compressibility, $\{\dot{\boldsymbol{f}}\}$ is equivalent nodal force vector, $\{f_u\}$ is a vector for elevation head. Furthermore, $[\mathrm{C}^*]$ is the damping matrix that results from imposition of the viscous boundary, and represents non-proportional damping. $[\mathrm{C}]$ is a matrix imposing a linear constraint on node movement, $\{\dot{\mu}\}$ is the Lagrangian undetermined multiplier, and $-[\mathrm{C}]^{\mathrm{T}}\{\dot{\mu}\}$ is a term with physical significance that acts as a constraint imposed on nodes.

Following the method of Foss (1958), we set

$$\{\dot{\boldsymbol{v}}\} = \{\boldsymbol{w}\} \tag{2}$$

The homogeneous form of equation (1) can be rewritten as

$$\begin{cases} [\mathrm{M}]\{\dot{\boldsymbol{w}}\} + [\mathrm{C}^*]\{\dot{\boldsymbol{v}}\} + [\mathrm{K}]\{\boldsymbol{v}\} - [\mathrm{L}]^{\mathrm{T}}\{\dot{u}\} - [\mathrm{C}]^{\mathrm{T}}\{\dot{\mu}\} = \{\boldsymbol{0}\} \\ [\mathrm{M}]\{\boldsymbol{w}\} - [\mathrm{M}]\{\dot{\boldsymbol{v}}\} = \{\boldsymbol{0}\} \\ [\mathrm{L}']\{\dot{\boldsymbol{v}}\} - [\mathrm{L}]\{\boldsymbol{v}\} + [\mathrm{H}]\{u\} + [\mathrm{G}]\{\dot{u}\} = \{\boldsymbol{0}\} \\ -[\mathrm{C}]\{\boldsymbol{v}\} = \{\boldsymbol{0}\} \end{cases} \tag{3}$$

Summarizing the system of simultaneous ordinary differential equations (3) in matrix form yields

$$[\mathrm{A}]\{\dot{\boldsymbol{x}}\} = [\mathrm{B}]\{\boldsymbol{x}\} \tag{4}$$

wherein,

$$\{\boldsymbol{x}\} = \begin{Bmatrix} \{\boldsymbol{v}\} \\ \{\boldsymbol{w}\} \\ \{u\} \\ \{\mu\} \end{Bmatrix}, \quad [\mathrm{A}] = \begin{bmatrix} [\mathrm{C}^*] & [\mathrm{M}] & -[\mathrm{L}]^{\mathrm{T}} & [\mathrm{O}] \\ [\mathrm{M}] & [\mathrm{O}] & [\mathrm{O}] & [\mathrm{O}] \\ [\mathrm{L}'] & [\mathrm{O}] & [\mathrm{G}] & [\mathrm{O}] \\ [\mathrm{O}] & [\mathrm{O}] & [\mathrm{O}] & [\mathrm{O}] \end{bmatrix},$$

$$[\mathrm{B}] = \begin{bmatrix} [\mathrm{K}] & [\mathrm{O}] & [\mathrm{O}] & -[\mathrm{C}]^{\mathrm{T}} \\ [\mathrm{O}] & -[\mathrm{M}] & [\mathrm{O}] & [\mathrm{O}] \\ -[\mathrm{L}] & [\mathrm{O}] & [\mathrm{H}] & [\mathrm{O}] \\ -[\mathrm{C}] & [\mathrm{O}] & [\mathrm{O}] & [\mathrm{O}] \end{bmatrix} \tag{5}$$

Assuming that $\{\boldsymbol{v}\} = \{\boldsymbol{v}_0\}e^{\lambda t}$, $\{u\} = \{u_0\}e^{\lambda t}$, and $\{\mu\} = \{\mu_0\}e^{\lambda t}$, we see that

$$\{\boldsymbol{x}\} = \{\boldsymbol{x}_0\}e^{\lambda t} \tag{6}$$

Here

$$\{\boldsymbol{x}_0\} = \{\{\boldsymbol{x}_0\}^{\mathrm{T}}\{\boldsymbol{w}_0\}^{\mathrm{T}}\{u_0\}^{\mathrm{T}}\{\dot{\mu}_0\}^{\mathrm{T}}\} \tag{7}$$

If an $\{\boldsymbol{x}\}$ such as that expressed in equation (6) exists, we arrive at the following general eigenvalue problem.

$$\lambda[\mathrm{A}]\{\boldsymbol{x}_0\} = [\mathrm{B}]\{\boldsymbol{x}_0\} \tag{8}$$

3 SIMULATION CONDITIONS

Calculations were performed under two-dimensional plane strain conditions. We examined the case of an embankment built on level ground. The finite element mesh and boundary conditions used for the calculations are presented in Figure 1. As boundary conditions for the ground, a viscous boundary (ρ=2.0g/cm^3,Vs=1000m/s) was imposed in the horizontal direction, a velocity boundary (fixed conditions) in the vertical direction along the lower-end face and a periodic boundary along the lateral faces of the ground. In addition, the lateral and lower-end faces of the ground were assumed to be undrained boundaries. The embankment, which was assumed to be saturated, was established by progressively adding elasto-plastic finite elements representing the two-phase soil-water in the location shown in Figure 1, and the simulation was continued until consolidation was completed. For the constitutive equation for the soil skeleton, we employed the elasto-plastic constitutive equation SYS Cam-clay model (Asaoka et al. 2002), which is

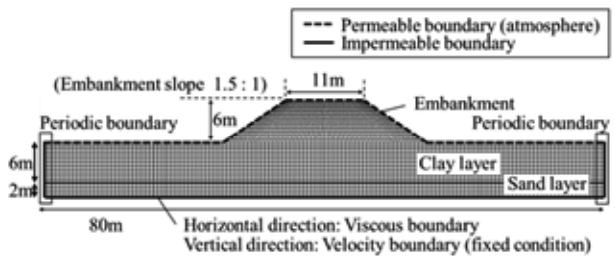

Figure 1. Finite element mesh and boundary condition

capable of describing the function of the skeleton structure. The sand in the lower portion of the ground was assigned a material constant corresponding to silica sand no. 6, and the overlying clay in the upper portion of the ground was assigned a material constant for *Tochi clay*. The embankment comprised a mixture of silica sand no. 7 and *Tochi clay* and was assigned a material constant for an intermediate soil (Noda et al. 2008b). The natural frequency and seismic response analyses of the soil structure-ground system after consolidation were analyzed under the above conditions.

4 INITIAL NATURAL FREQUENCY AND NATURAL FREQUENCY MODE OF THE SOIL STRUCTURE-GROUND SYSTEM

The initial (the post consolidation) natural frequency modes causing large-scale deformation of the ground (MODE 1) and large-scale deformation of the embankment (MODE 2) yielded by our calculations are presented in Figure 2. Although the natural frequency mode in our analytical approach is expressed as a linear combination of the real and imaginary parts of the complex eigenvector, here we only show the mode expressed by the imaginary part.

(a) MODE 1: Large scale deformation of ground

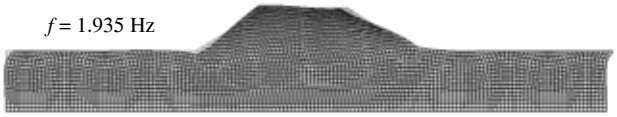

(b) MODE 2: Large scale deformation of embankment

Figure 2. Natural frequencies and natural frequency modes (imaginary part)

5 SEISMIC RESPONSE ANALYSIS OF GROUND WITH AN OVERLYING EMBANKMENT

Our analyses were performed on the post consolidation soil structure-ground system described in the previous section. The input seismic waves had dominant frequencies close to the natural frequencies of the system as a whole, and their magnitudes were adjusted to generate a maximum acceleration of 200 gal. The acceleration history and Fourier amplitude spectrum of the input waves are shown in Figure 3.

WAVE 1 represents a seismic wave with a dominant frequency equal to the natural frequency of MODE 1, and WAVE 2 represents a seismic wave with a dominant frequency equal to the natural frequency of MODE 2. After inputting these seismic waves into all the nodes at the bottom face of the ground representing the horizontal viscous boundary, the simulation was allowed to run until consolidation of the ground stopped. The inputs of WAVE 1 and WAVE 2 are referred to below as CASE 1 and CASE 2.

The changes in the shear stress distribution during and after the simulated earthquake are presented in Figure 4. It is evident that in both CASE 1 and CASE 2, delayed failure occurred after the earthquake. Examining the progression of the shear stress, it can be seen that in CASE 1, a slip surface (strain localized area) extending from the top of the sand layer to the middle of the ground developed during the earthquake. Thereafter, the slip surface continued to expand over time from the ground to the embankment, ultimately resulting in delayed failure. Meanwhile, in CASE 2, although strain was localized at the top of the sand layer, no large-scale deformation of either the embankment or the ground occurred during the earthquake.

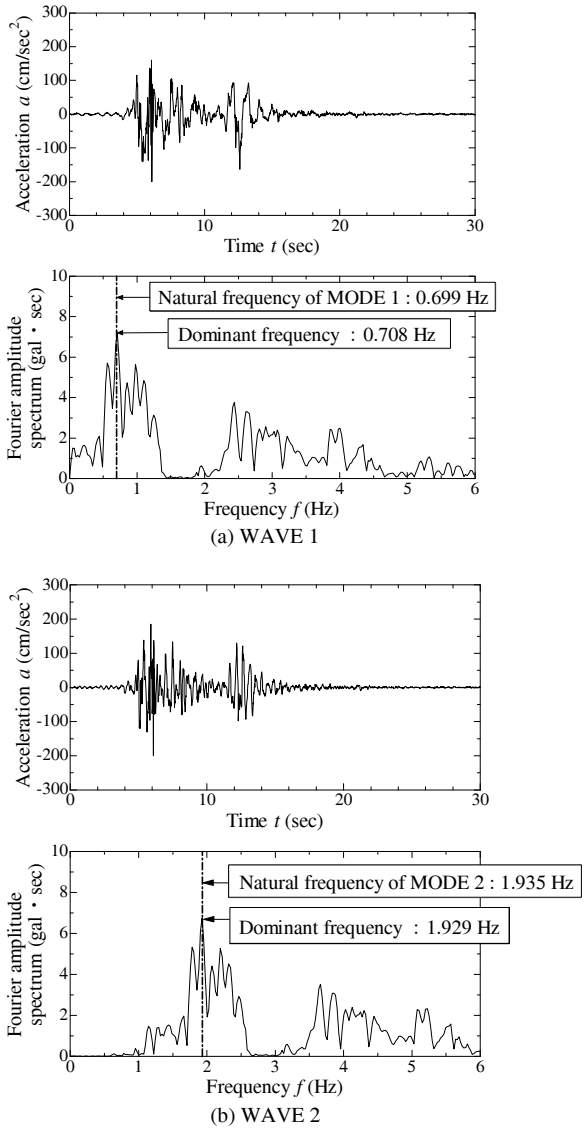

Figure 3. Acceleration wave form and Fourier amplitude spectrum of input seismic waves

However, with the progress of time, a slip surface developed in the embankment and subsequently expanded into the ground. That is, we observed a significant difference in the delayed failure behavior of the soil structure-ground system depending on the dominant frequency of the seismic wave.

In order to elucidate the reason for this difference in the progression of delayed failure, we first investigated the differences in vibration characteristics during the earthquake in the two cases. The Fourier amplitude spectrum of the acceleration response for the layer boundary at the center of the ground is presented in Figure 5. We see that in CASE 1, the frequency component that was close to the dominant frequency of WAVE 1 underwent substantial amplification at the top of the clay layer as the seismic wave passed from the ground to the embankment, and that this area experienced resonance corresponding to MODE 1 (upper panel of Figure 2), which caused large-scale deformation of the clay layer. In CASE 2, the frequency component that was close to the dominant frequency of WAVE 2 underwent substantial amplification at the crown of the embankment and the embankment experienced resonance corresponding to MODE 2 (lower panel of Figure 2) that caused large-scale deformation of the embankment.

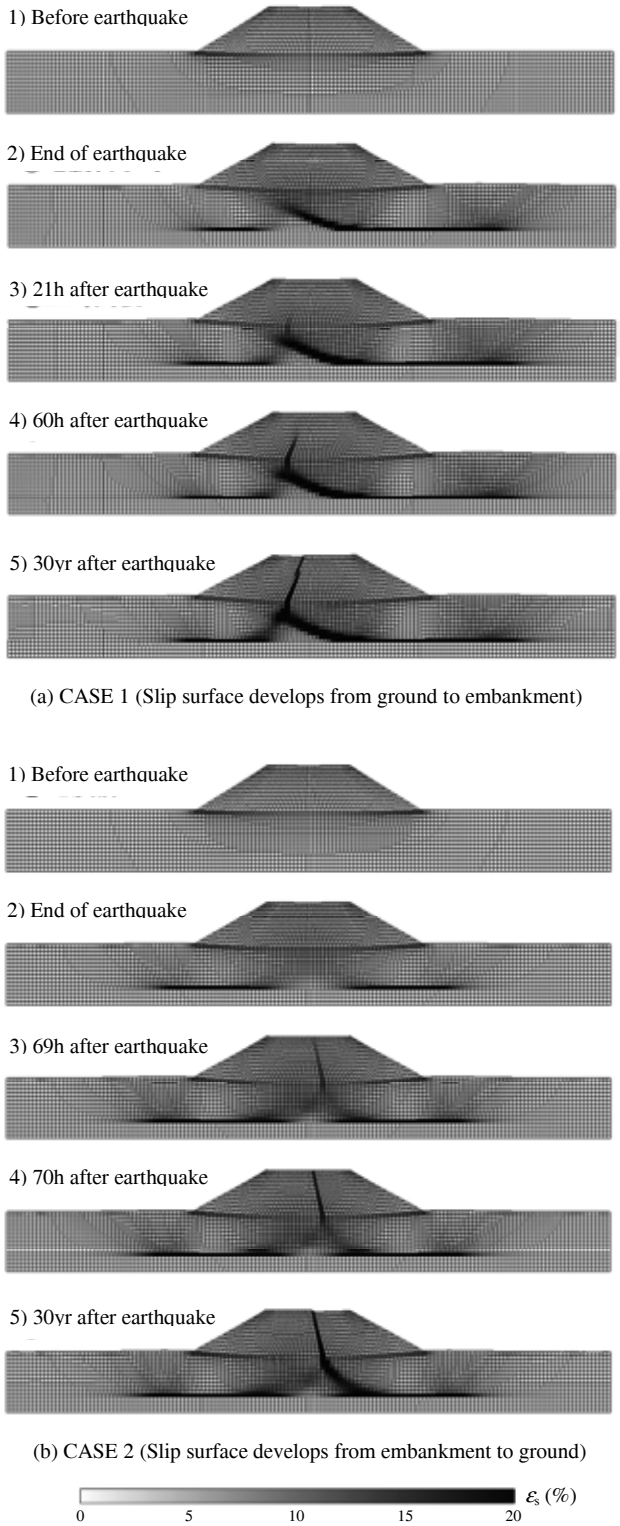

Figure 4. Shear strain distributions

Next, we investigated the mechanisms underlying the delayed failures observed in our simulations. The distribution of excess pore water pressure when the earthquake stopped is presented in Figure 6. It can be seen that, in both cases, the upper portion of the ground and inside the embankment experienced a negative excess pore water pressure, while the central to lower portions of the ground experienced positive excess pore water pressure. Because the upper portion of the ground and the embankment were in an overconsolidated state prior to the earthquake, when subjected to undrained shear

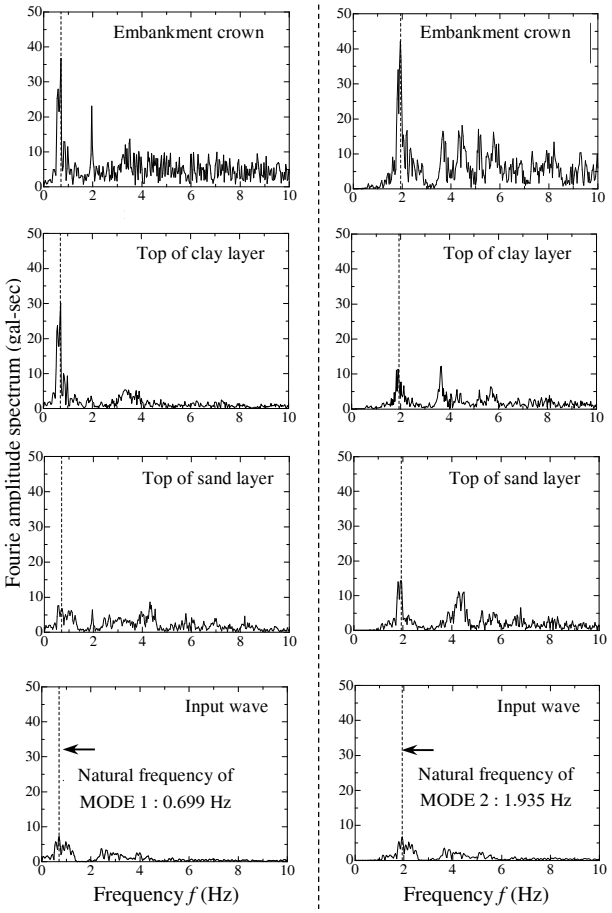

(a) CASE 1 (b) CASE 2

Figure 5. Fourier amplitude spectra of acceleration response

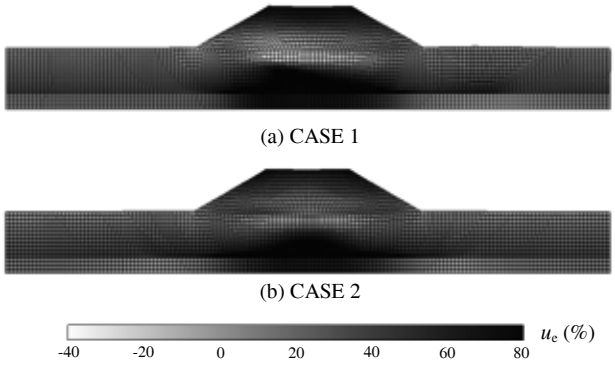

(a) CASE 1

(b) CASE 2

Figure 6. Distribution of excess pore water pressure at the end of the earthquake

during the earthquake, they underwent hardening accompanied by plastic volumetric expansion, which resulted in negative excess pore water pressure. Meanwhile, because the lower portion of the ground was in a nearly normally consolidated state of consolidation prior to the earthquake, when subjected to undrained shear during the earthquake, it underwent hardening accompanied by plastic compression, which resulted in positive excess pore water pressure. Although the data are not presented here due to space limitations, these behaviors can be confirmed by examining the actual behavior of the soil elements. Following the earthquake, in the process of returning to the steady state of pore water pressure, the soil elements in the upper ground layers, which exhibited negative excess pore water pressure, absorbed water from the surrounding soil elements, resulting in softening and, ultimately, the delayed failure occurred. While this mechanism of delayed failure applies to both CASE 1 and CASE 2, the substantial difference in the progression of delayed failure shown in Figure 4 arises from the difference in the dominant natural frequency mode between CASE 1 and CASE 2. In CASE 1, because the system resonated in MODE 1 (upper panel in Figure 2) during the earthquake, the shear stress first became localized in the ground and the slip surface progressively expanded from the upper portion of the ground to the embankment as a result of softening due to water absorption. Meanwhile, in CASE 2, because the system resonated in MODE 2 (lower panel in Figure 2) during the earthquake, the embankment experienced high-amplitude shaking while the ground did not. For this reason, after the earthquake, slip failure resulting from softening due to water absorption occurred first in the embankment. The loss of equilibrium of force in the embankment induced shear in the ground components directly under the embankment, which led to the development of a slip surface in the ground.

6 CONCLUSIONS

In this paper, we proposed a method for calculating the natural frequency and natural frequency mode in the context of an initial-boundary value problem for the ground. In addition, we demonstrated through seismic response analyses of a soil structure-ground system that seismic motions with different dominant frequencies result in different dominant natural frequency modes. We further showed that the progression of ground deformation, including delayed failure, following an earthquake is strongly influenced by this natural frequency mode. In considering initial-boundary value problems of elasto-plastic materials that are based on finite deformation theory, although such materials have non-linear geometric and material properties and their natural frequencies change from moment to moment, it is still important to understand their natural frequencies and natural frequency modes, even if only for the initial state. Finally, although the simulations presented here used only seismic waves with dominant frequencies close to the natural frequencies of the system, we have confirmed that the input of seismic waves of a similar magnitude but with dominant frequencies far from the natural frequencies does not result in significant deformation during earthquakes or subsequent delayed failure.

7 REFERENCES

Noda, T., Asaoka, A. and Nakano, M. 2008a. Soil-water coupled finite deformation analysis based on a rate-type equation of motion incorporating the SYS Cam-slay model, *Soils and Foundations*, 45(6), 771-790.

Christian, J. T. 1968. Undrained stress distribution by numerical method, *Proc. ASCE*, 94, 1331-1345.

Akai, K. and Tamura, T. 1978. Numerical analysis of multi-dimensional consolidation accompanied with elasto-plastic constitutive equation, *Journal of JSCE*, 269, 95-104.

Asaoka, A., Noda, T. and Kaneda, K. 1998. Displacement/traction boundary conditions represented by constraint conditions on velocity field of soil, *Soils and Foundations*, 38(4), 173-181.

Foss, K, A. 1958. Coordinates which Uncouple the Equations of Motion of Damped Linear Dynamic Systems, *Journal of Applied Mechanics*, ASME, 32(3), 361-364.

Noda, T. Nakai, K. and Asaoka, A. 2008b. Delayed failure of a clay foundation-embankment system after the occurrence of an earthquake, *Theoretical and applied mechanics JAPAN*, 57, 41-47.

Asaoka, A., Noda, T., Yamada, E., Kaneda, K. and Nakano, M. 2002. An elasto-plastic description of two distinct volume change mechanisms of soils, *Soils and Foundations*, 42(5), 47-57.